Insight into acetylene plasma deposition using molecular dynamics simulations

Pascal Brault, Marisol Ji, Dario Sciacqua, Fabienne Poncin-Epaillard, Johannes Berndt, Eva Kovacevic

Molecular dynamics simulations of acetylene plasma deposition of polymer films.

P. Brault[1,*], M. Ji[2], D. Sciacqua[1], F. Poncin-Epaillard[2], J. Berndt[1], E. Kovacevic[1]

[1]GREMI, CNRS - Université d'Orléans BP6744, 45067 Orléans cedex 2, France
[2]Institut des Molécules et Matériaux du Mans, Le Mans Université – CNRS, Avenue Olivier Messiaen, 72085 Le Mans, France

*Correspondence
Pascal Brault, GREMI, CNRS - Université d'Orléans BP6744, 45067 Orléans cedex 2, France
Email: pascal.brault@univ-orleans.fr

_____

Abstract: Molecular dynamics simulations are carried out for studying growth and properties of polymers from pure acetylene plasma. Mixture of H, C_2H and C_2H_2 is the initial composition for running the molecular dynamics simulations. Resulting films are characterized by characterizing bond order, [H]/[C] ratio and simulated infrared spectrum. The latter is qualitatively compared with three different experiments: IR peak identification and positions are recovered.

keywords: Molecular dynamics; plasma deposition; plasma polymer; polymer film

1 INTRODUCTION

The use of plasmas for the deposition of thin films - often subsumed under the term plasma-assisted chemical vapor deposition or PECVD - has a long history. In particular low temperature plasmas have found numerous applications ranging from the production of wear resistance and antireflection coatings to the deposition of organic layers in microelectronics. The advantages of deposition techniques based on such plasmas include the possibility to deposit films at moderate temperatures and the conformal coating of complex surface structures (e.g. sidewalls in microelectronic components). An additional advantage of PECVD techniques is their flexibility when it comes to the choice of gases used for the deposition process. Silane for example has been frequently used for the deposition of silicon in semiconductor industry, whereas gases like e.g. methane, acetylene, benzene or even more complex molecules as aniline can be easily used for the production of carbon based deposits.

The breakdown of the initial monomer molecules by electron impact dissociation is the first step in each PECVD process and is responsible for the creation of a great variety of different radicals and positive (and sometimes negative) ions. Depending on the nature of the monomer the complexity of the system can be further increased by subsequent polymerization reactions in the plasma volume which will lead to the formation of larger molecules and sometimes even to the formation of nanoparticles (see e.g. [1,2] for the case of acetylene). Since all these molecules (and atoms like e.g. H-atoms) contribute to the species flux arriving at surfaces exposed to the plasma it is often difficult to identify specific radicals as being responsible for the growth of thin films. This is even more so since the synergistic interplay of different molecules can strongly influence the growth process and since the exact composition of the species flux strongly depends on external discharge parameters like pressure, power, gas flow and so on. And even from a purely experimental point of view it is a very challenging (nearly impossible) task to get a (complete) quantitative description of the composition of the species flux arriving at a substrate. Moreover, a complete description would also require the knowledge of the ion energy distribution function of all positive ions reaching the surface since the kinetic energy of these ions play a fundamental role in the deposition process and for the properties of the resulting thin films. Not least the great dimension of the parameter space (power, pressure, gas flow, pumping speed, pulse frequency and duty cycle, geometrical dimensions) renders complete systematic parameter studies impossible. A more targeted control of PECVD techniques with respect to the production of thin films with tailored properties requires therefore approaches that go beyond simple experimental trial and error procedures. A possible different

approach is to combine experimental observations and simulation techniques as for example Molecular dynamics (MD).

In this contribution we will focus on the growth of thin films from acetylene plasmas and how this process can be viewed from a Molecular Dynamics point of view. Molecular dynamics (MD) simulation technique is a powerful tool for examining plasma reactive processes at surfaces [3, 4]. Such a technique only requires knowledge of interatomic forcefields, positions and velocities initial conditions (ideally reflecting experimental conditions [5]). reactive forcefields are mandatory in the case of polymer film growth since the growth results from bond breaking/formation elementary processes at the surface and on the growing film. Fortunately, in the case of hydrocarbon molecules and radicals numerous reactive relevant forcefields are available. The simplest and computationally fast is the REBO (Reactive Empirical Bond Order) potential [6]. Another version called AIREBO is including long range and torsional forces [7]. Another forcefield class is including dynamics of partial charges in addition to bond order: variable charge reactive forcefields. The most used forcefields of this class are: COMB and ReaxFF [8]. Recent work compared REBO, AIREBO and ReaxFF potential for hydrocarbon radical deposition onto silver substrate [9]. Since in this study, REBO force field was determined to be the most relevant, we adopt the REBO forcefield.

The present work is dedicated to MD simulations deposition and growth of polymer films on stainless steel 306L substrate. Sticking coefficient of individual selected species, of mixture are calculated and presented in the results and discussion section. H content both in film and in substrate are determined as well as the [H]/[C] content. A typical IR spectrum of a resulting film is simulated and compared to three different experimental results.

2 MODELING AND EXPERIMENTS

2.1 Molecular dynamics simulations

Simulated depositions are carried out on a stainless steel 306 hcp (100) oriented slab with composition $Fe_{67}Cr_{17}Ni_{14}Mo_2$. The substrate size is 80.36 x 80.36 x 14.35 $Å^3$. 10000 species are released toward the surface every 2 ps from region located between 20 and 120 Å above the substrate. For the study we have selected C_2H as the main radical and then prepare a vapor with 10000 species shared as 25% C_2H, 25% H and 50% C_2H_2. No CH and no C_2 were included. The molecular motions are calculated in the NVE ensemble (thus, without any constraint) while the substrate is constrained to keep its temperature constant using NVT dynamics. The damping time for dissipating bond formation energy through the substrate is 10 fs while the timestep for solving the equation of motion is 0.25 fs. When a radical is

reacting to the already existing film, the energy is kept free to be distributed along the freedom degrees before being dissipated to the substrate. Thus, there is no other thermostat than the substrate.

Since molecular dynamics is a method solving Newton equation of motion, it only requires the knowledge of the interatomic forces as well as position and initial conditions of all species. The initial velocities are randomly chosen from a Maxwell-Boltzmann temperature of 300K since initial position of acetylene monomers and radicals are randomly chosen in the deposition region above the substrate.

Following the study revealing that REBO potential is most suited, since it is better consistent with density functional simulations, for such an hydrocarbon film growth [9], we use it in this work.

Basically, REBO potential is a bond order potential with an analytic form derived from pseudo potential theory of Abell [10] and which reads:

$$E_b = \sum_i \sum_{j>i} \left[V_R(r_{ij}) - b_{ij} V_A(r_{ij}) \right]$$

where V_R, V_A are the pair repulsive and attractive part of the interatomic potential, while b_{ij} stands for the bond order term and r_{ij} is the interatomic distance between atom i and j.

The functional forms of V_R and V_A pair terms are given by [4]:

$$V_R(r) = f_c \left(1 + \frac{Q}{r}\right) A e^{-\alpha r}$$

$$V_A(r) = f_c \sum_{n=1}^{3} B_n e^{-\beta_n r}$$

f_c is a cutoff function limiting the range of the covalent bonds. A, B_n, α, β_n are the parameters of the Morse function and Q the parameter of the screened Coulomb term.

The bond order term b_{ij} allows capturing the local coordination behavior and thus can reproduce the reaction with the right bonding breaking/formation. For example, only H atoms can be bonded to a carbon. Moreover, the sp character is distance dependent. Full computing details of the b_{ij} term are available in Ref. 6.

Metal atom motions in the stainless-steel substrate are described by Embedded Atom Method [11-13].

The EAM potential is a many-body potential which is including the collective motions of electrons. Essentially, each atom contributes to the overall charge density of the system, via a spherical electron charge, centered at its nucleus. The binding between atoms is modelled

considering that these atoms are embedded in this “pool” of charge, where the energy gained by embedding an atom at location *r* is a function of the local electron density.

The EAM potential energy *E* of the system thus reads as:

$$E = \frac{1}{2}\sum_{i,j\neq i} \varphi_{ij}\,(r_{ij}) + \sum_{i} F_i(\rho_i)$$

where E_i is the potential energy of an atom i, $\varphi(r_{ij})$ is the pair energy term as a function of the interatomic separation r_{ij} between atoms i and j, and $F_i(\rho_i)$ is the many-body embedding energy term, function of the local electron density, ρ_i, at the position of atom i.

The local electron density is calculated as:

$$\rho_i = \sum_{j,j\neq i}^{N} f_j(r_{ij}) \qquad (3)$$

where $f_j(r_{ij})$ is the contribution from atom j to the electron density at the site of the atom i.

The pair potential energy term is defined as:

$$\varphi(r) = \frac{A\exp\left[-\alpha\left(\frac{r}{r_e}-1\right)\right]}{1+\left(\frac{r}{r_e}-\kappa\right)^{20}} - \frac{B\exp\left[-\beta\left(\frac{r}{r_e}-1\right)\right]}{1+\left(\frac{r}{r_e}-\lambda\right)^{20}}$$

where r_e is the equilibrium spacing between nearest neighbors, A, B, α, and β are four adjustable parameters, and κ and λ are two additional parameters for the cutoff distances [12,13]. The electron density function is taken to have the same form as the attractive term in the pair potential with the same values.

The electron density function is given by:

$$f(r) = \frac{f_e\exp\left[-\beta\left(\frac{r}{r_e}-1\right)\right]}{1+\left(\frac{r}{r_e}-\lambda\right)^{20}}$$

The pair potential between atoms of two different elements (a and b) is built using the mixing rule [14]:

$$\varphi^{ab}(r) = \frac{1}{2}\left[\frac{f^b(r)}{f^a(r)}\varphi^{aa}(r) + \frac{f^a(r)}{f^b(r)}\varphi^{bb}(r)\right]$$

The embedding energy function F(□) is represented by three equations defining it in different electron density ranges and having matching values and slopes at the two junctions:

$$F(\rho) = \sum_{i=0}^{3} F_{ni}\left(\frac{\rho}{0.85\rho_e}-1\right)^i, \quad \rho < 0.85\rho_e$$

$$F(\rho) = \sum_{i=0}^{3} F_i \left(\frac{\rho}{\rho_e} - 1\right)^i, \quad 0.85\rho_e \leq \rho < 1.15\rho_e$$

$$F(\rho) = F_e \left[1 - \eta \ln\left(\frac{\rho}{\rho_e}\right)\right] \times \left(\frac{\rho}{\rho_e}\right)^{\eta}, \quad \rho \geq 1.15\rho_e$$

where η, F_i, F_{ni}, F_e, ρ_e are adjustable EAM parameters [11, 13]. The substrate has been built from a Fe bcc structure with randomly replacing Fe atoms by Cr, Ni and Mo at the desired composition, say $Fe_{67}Cr_{17}Ni_{14}Mo_2$ here. Necessary potential parameters for building the forcefield of this alloy can be found in Ref. 12

Interaction potentials of C and H with the stainless-steel atoms are modeled by Lennard-Jones functions:

$$V_{LJ}(r_{ij}) = 4\varepsilon_{ij}\left[\left(\frac{\sigma_{ij}}{r_{ij}}\right)^{12} - \left(\frac{\sigma_{ij}}{r_{ij}}\right)^{6}\right]$$

with r_{ij} is the interatomic distance between atoms i and j. σ_{ij} and ε_{ij} are the Lennard-Jones parameters: range and well depth between atoms i and j. When σ_{ii} and ε_{ii} are known, the Lorenz-Berthelot mixing rules apply: $\sigma_{ij} = \frac{\sigma_{ii}+\sigma_{jj}}{2}$ and $\epsilon_{ij} = \sqrt{\epsilon_{ii}.\epsilon_{jj}}$.

σ_{ij} and ε_{ij} values are summarized in **Table 1**.

TABLE 1. Lennard-Jones parameter of interactions between Fe, Cr, Ni, Mo, C and H [9, 14, 15, 16]

atom pair	σ (Å)	ε (eV)	atom pair	σ (Å)	ε (eV)	atom pair	σ (Å)	ε (eV)
Cr-Cr	3.6	0.215	Cr-C	3.50	0.0228	Cr-H	2.52	0.0066
Fe-Fe	2.327	0.527	Fe-C	2.86	0.0356	Fe-H	1.88	0.0103
Mo-Mo	2.551	0.838	Mo-C	2.98	0.0449	Mo-H	1.99	0.0129
Ni-Ni	2.282	0.52	Ni-C	2.84	0.0354	Ni-H	1.86	0.0102
C-C	3.4	$2.41\ 10^{-3}$						
H-H	1.436	$2.00\ 10^{-4}$						

The molecular dynamics simulations are carried out over $20\ 10^6$ timesteps (0.5 ns) using the LAMMPS software [15, 16].

2.2 Acetylene plasma film deposition and characterization

Plasma polymerization experiments were performed in a capacitive radio-frequency (RF, 13.56 MHz) plasma reactor. The low pressure is maintained using to a turbomolecular pump (Alcatel ATP-80) coupled with a primary rotary pump. Typical residual pressures are maintained between 10^{-5} and 10^{-4} mbar, while the working pressure is kept around 10^{-2} mbar and measure by a wide range capacitive-penning pressure gauge (Alcatel ACC 1009). The glow discharge is injected between two parallel electrodes separated by a fixed distance of 12 cm, and powered with a Caesar RF generator (Advanced Energy), with powers ranging from 5 to 100 W. Reflected power was kept minimum using to a RF Navio matchbox (Advanced Energy). Plasma discharges were performed in pulse wave (t_{off} from 18 to 184 µs, t_{on} maintained at 17 µs, *d.c* from 8 to 50 and *f* from 5 kHz to 30 kHz). Plasma discharges were created in acetylene (Air Liquide, with no further purification) atmosphere whose flow rates (Q) varies from 10 to 40 sccm, with a constant working pressure of 1.0 10^{-2} mbar.

FTIR spectroscopy

Chemical composition of the plasma polymer films (pp-Ac) deposited on transparent KBr pellets was extracted from Bruker Vertex 70 v spectrometer with 2 cm^{-1} resolution in the range 4000 - 400 cm^{-1}, 40 scans were recorded under vacuum. The FTIR spectra were done 10 min after the sample deposition. Spectral data were treated with Opus software for baseline correction and CO_2/H_2O subtraction.

In order to demonstrate the impact of external parameters and discharge configuration on the thin film characteristics a second plasma source was employed for the deposition of thin films from an acetylene plasma. In this case the capacitively coupled plasma (a GEC type reactor [17]) was operated at a pressure of 0.20 mbar with a flow of 10 sccm of acetylene. The plasma was pulsed with a frequency of 25 Hz and a duty cycle of 0.25 and an averaged rf-power of approximately 3 Watt. Two deposition experiments were carried out with these discharge parameters. In the first case the silicon wafer (on which the film was deposited) was placed on the grounded electrode, in the second case it was placed on the powered electrode. The infrared absorption spectra of both films were also measured by means of a Bruker FTIR spectrometer with 2 cm^{-1} resolution in the range from 1000 to 4000 cm^{-1}. **Table 2** summarizes all experimental conditions.

TABLE 2. Experimental plasma deposition conditions.

Sample	**C_2H_2 flow (sccm)**	**Pressure (mbar)**	**Support electrode**
A	10	0.01	grounded
B	10	0.2	powered

C	10	0.2	grounded

3 RESULTS AND DISCUSSION

Figure 1 shows the final deposition of the H, C_2H and C_2H_2 mixture after 0.5 ns. The film exhibit connected C_xH_y long chains.

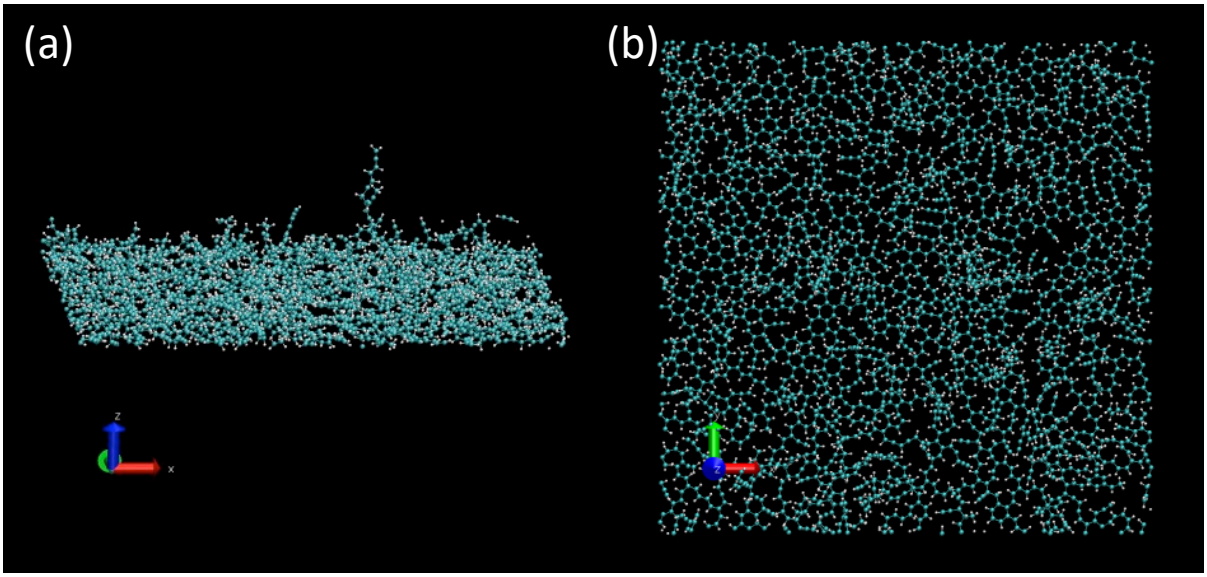

FIGURE 1. Final snapshots (balls and sticks) of a typical polymer film. (a) side view (b) top view. Blue balls are carbon atoms while white are Hydrogen atoms

The [H/C] ratio of the films are of order of 0.8. The carbon single, double and triple bond ratios are 20, 75 and 5 % as calculated from the film radial distribution function. Corresponding average bond lengths are respectively 1.54 ± 0.04 Å, 1.40 ± 0.03 Å, 1.21 ± 0.03 Å. These results are summarized in **Table 3**.

TABLE 3: Bond order fractions and average bond length of the typical film of Fig. 1

C- C bond type	**single**	**double**	**triple**
ratio (%)	20	75	5
bond length (Å)	1.54 ± 0.04	1.40 ± 0.03	1.21 ± 0.03

For direct comparison with FTIR experiments, the infrared spectrum of the simulated film of Figure 1, was calculated using DFTB3 [18] scheme with the 3ob parametrization. The

calculations have been carried out using the Amsterdam Modeling Suite [19, 20]. **Figure 2** displays both experimental and simulated spectra.

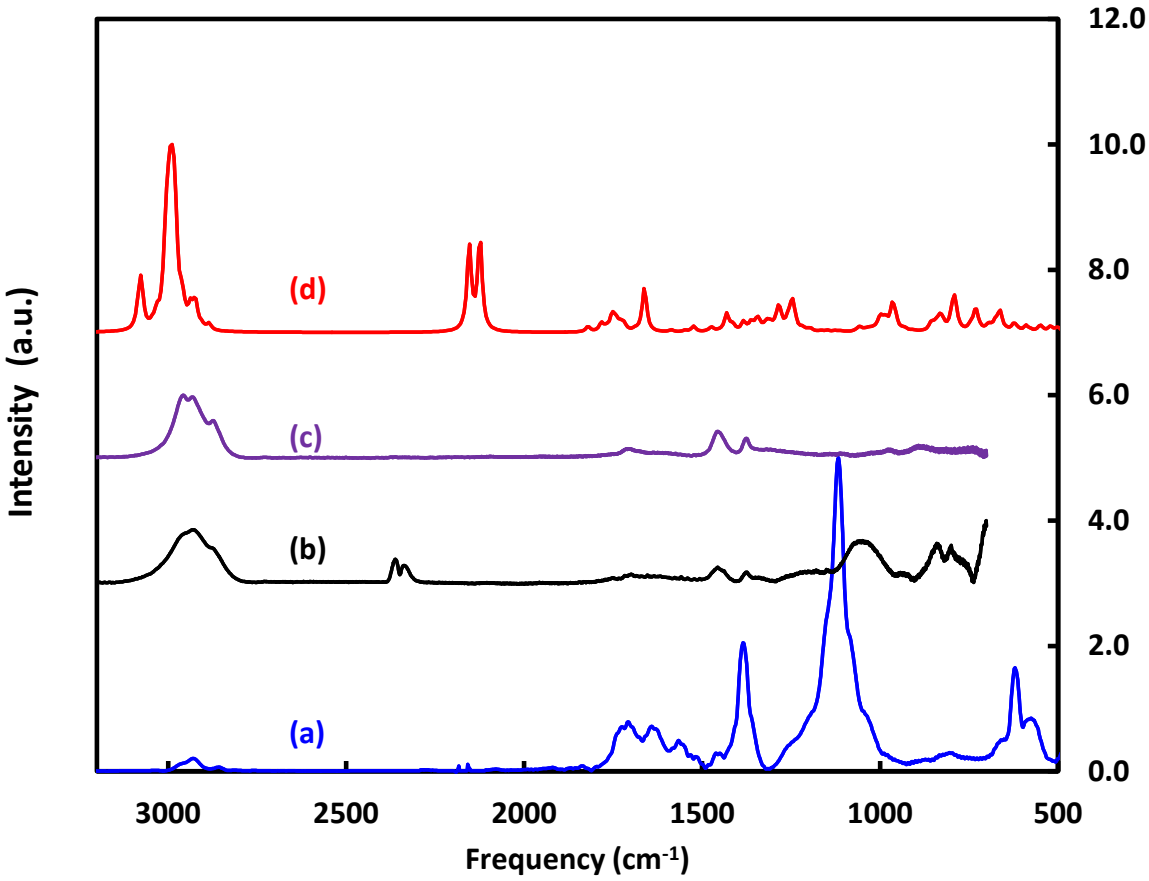

FIGURE 2. IR spectra FTIR measurement of (a) experiment A, (b) experiment B, (c) experiment C (defined in Table 2 and (d) simulated IR spectrum from film displayed in Figure 1. Each spectrum is normalized to its maximum.

Experimental FTIR spectroscopy characterization was performed in transmission mode. **Table 4** and Figure 2 (a-c) are summarizing all the experimental FTIR data. A comparison between the different experimental FTIR spectra shows that the relative intensity of the individual absorption peaks depends on the experimental conditions under which the thin films were deposited. The peak positions, however, are less effected by the experimental conditions.

Table 4: Assignment of pp-Ac FTIR vibrational modes

Wavenumber (cm^{-1})	**pp-Ac experiments**	**pp - Ac simulated**
3442	*v* O-H from H_2O	no
2965	*v*(asym) CH_3	yes

2925	ν(asym) CH_2	yes
2856	ν(sym) CH_2	yes
1720	ν C=O	no
2125/2124	yes (small)	C=C-C linear antisym
1645	ν C=C	yes
1463	δ CH_2	yes
1387	δ (sym) CH_3	yes
1084/1120	ν C-C (only A)	no
659	δ C-H from C=C	yes

All the spectra present the vibration bands of CH_x or C-C bonds. The signature of specific functional group of the precursor is noticed (C-C double bond and carbonyl). Pp-Ac is oxidized since C-O, C=O or C-OH are assigned, such oxidation corresponds to the dangling radicals formed during the plasma polymerization that age after the treatment [21, 22]. However, with pp-Ac, this post-oxidation is less pronounced than observed in [21] mostly since the storage duration after the deposition and before the FTIR analyze is shorter, few minutes versus two hours. Moreover, such oxidation may be also assigned to oxygen / water desorption from chamber wall or to acetone plasma fragmentation. Indeed, this molecule is added in the acetylene bottle for safety storage and was interfering in some surface modification [23].
When looking at the simulated spectrum (Figure 2(d)), the HO mode of H_2O mode around 3500 cm-1 is not present since no oxygen related species are included in the MD simulations. On the other hand, a peak at 2160 cm^{-2} related to C-C=C Q2 stretching mode is appearing. This mode is also present in experiment A but not in experiments B and C. Also appearing in experiments B and not in experiments A, C and simulation is the presence of CO_2 line at 1360 cm-1 is related to CO_2 contamination. On the lower frequency part, below 2000 cm^{-1}, the agreement is qualitatively good in showing both C=C and C-C modes reported in Table 3. The mixture of these bonds appearing around 3000 cm^{-1} is also common to experiments and simulations. Intensities are very different and are dependent on experimental conditions. Experiment A differs from B and C ones by pressure and electrodes arrangements and thus delivered power densities. A detailed study of the influence of experimental conditions is dedicated to a futher work, since the present work is aiming at showing capability of MD simulations in reproducing IR spectrum of plasma polymer films. This dependence on plasma deposition conditions implies that initial conditions for MD simulations should be adapted to

the targeted experiment. Especially, plasma composition (plasma produced radicals) should be precisely determined for serving as input for directly comparable MD simulations

4 CONCLUSION

Molecular dynamics simulations have been carried out on for studying growth of acetylene plasma deposition mimicked by a composition including H, C_2H radical and C_2H_2 molecule. The amount of C=C double bond in the simulated deposited film is 75%. IR spectra of acetylene plasma deposited film is recorded and compared to the simulated one corresponding to MD film deposition. Except band originating from residual water, and CO resulting from water interaction with the film (since no water is included in simulations), the agreement is qualitatively good (peak identification and positions) for C=C and C-H modes. Nevertheless, a C-C single bond mode is lacking in the simulated spectrum. This comes from the high C=C double bond content generated by the simulation conditions. Intensities cannot be directly compared, due to the different plasma deposition conditions, etc.

ACKNOWLEDGEMENT

Project ANR-17-CE08-0018 PLASMA-BOND funding is greatly acknowledged.

REFERENCES

[1] S. Stoykov, C. Eggs, U. Kortshagen, Plasma chemistry and growth of nanosized particles in a C_2H_2 RF discharge, *J. Phys. D: Appl. Phys.* **34** (2001) 2160.

[2] Ch. Deschenaux, A. Affolter, D. Magni, Ch. Holleinstein, P. Fayet, Investigations of CH_4, C_2H_2 and C_2H_4 dusty RF plasmas by means of FTIR absorption spectroscopy and mass spectrometry, *J. Phys. D: Appl. Phys.* **32** (1999) 1876

[3] D. B. Graves, P. Brault, Molecular dynamics for low temperature plasma-surface interaction studies, *J. Phys. D* **42** (2009) 194011

[4] E. Neyts, P. Brault, Molecular dynamics simulations for plasma surface interactions, *Plasma Processes and Polymers* **14** (2017) 1600145

[5] P.Brault, Multiscale Molecular Dynamics Simulation of Plasma Processing: Application to Plasma Sputtering, *Front. Phys.* **6** (2018) 59

[6] D. W. Brenner, O. A. Shenderova, J. A. Harrison, S. J. Stuart, B. Ni, S. B. Sinnott, A second-generation reactive empirical bond order (REBO) potential energy expression for hydrocarbons, *J Physics: Condensed Matter* **14** (2002) 783-802

[7] S. J. Stuart, A. B. Tutein, J. A. Harrison, A reactive potential for hydrocarbons with intermolecular interactions, *J. Chem. Phys.* **112** (2000) 6472-6486

[8] T. Liang, Y.K. Shin, Y. T. Cheng, D. E. Yilmaz, K. G. Vishnu, O. Verners, C. Zou, S. R.Phillpot, S. B. Sinnott, A. C. T. van Duin, Reactive Potentials for advanced atomistic simulations. *Annu. Rev. Mater. Sci.* **43** (2013) 109-129

[9] M. Zarshenas, K. Moshkunov, B. Czerwinski, T. Leyssens, A. Delcorte, Molecular dynamics simulations of hydrocarbon film growth from acetylene monomers and radicals: Effect of substrate temperature, *J. Phys. Chem C* **122** (2018) 15252 - 15263

[10] G. C. Abell, Empirical chemical pseudopotential theory of molecular and metallic bonding, *Phys. Rev. B* **31** (1985) 6184

[11] S. Foiles, M. Baskes, M. Daw, Embedded-atom-method functions for the fcc metals Cu, Ag, Au, Ni, Pd, Pt, and their alloys, *Phys. Rev. B* **33** (1986) 7983-7991.

[12] X. W. Zhou, R. A. Johnson, and H. N. G. Wadley, Misfit-energy-increasing dislocations in vapor-deposited CoFe/NiFe multilayers, *Phys. Rev. B* **69** (2004) 144113

[13] X. W. Zhou, H. N. G. Wadley, R. A. Johnson, D. J. Larson, N. Tabat, A. Cerezo, A. K. Petford-Long, G. D. W. Smith, P. H. Clifton, R. L. Martens and T. F. Kelly, Atomic scale structure of sputtered metal multilayers, *Acta Materialia* **49** (2001) 4005–4015

[14] R. A. Johnson, Alloy models with the embedded-atom method, *Phys. Rev. B* **39** (1989) 12554-12559

[15] S. Plimpton, Fast parallel algorithms for short-range molecular dynamics, *Journal of Computational Physics* **117** (1995) 1-19

[16] available at URL: http://lammps.sandia.gov/

[17] D. P. Lymberopoulos, D. J. Economou, Two-Dimensional Self-Consistent Radio Frequency Plasma Simulation Relevant to the Gaseous Electronics Conference RF Reference Cell, *J. Res. Natl. Inst. Stand. Technol.* **100** (1995) 473

[18] M. Gaus, Q. Cui, M. Elstner, DFTB3: Extension of the self-consistent-charge density-functional tight-binding method (SCC-DFTB), *J Chem Theory Comput.* **7** (2012) 931-948.

[19] G. te Velde, F. M. Bickelhaupt, E. J. Baerends, C. Fonseca Guerra, S. J. A. van Gisbergen, J. G. Snijders, and T. Ziegler, "Chemistry with ADF," *J. Comput. Chem.* **22** (2001) 931

[20] ADF 2019. 3 and AMS 2020.1, SCM, Theoretical Chemistry, Vrije Universiteit, Amsterdam, The Netherlands. See http://www.scm.com.

[21] I. Retzko, J. F. Friedrich, A. Lippitz, W. E. S.Unger, Chemical analysis of plasma-polymerized films: the application of X-Ray photoelectron spectroscopy (XPS), X-Ray

absorption spectroscopy (NEXAFS) and fourier transform infrared spectroscopy (FTIR). J. *Electron Spectrosc. Relat. Phenom.* **121** (2001) 111-129.
[22] A. M. de Oliveira Neto, W. H. Schreiner, J. F. Justo, A. M. de Oliveira, E. C. Rangel, S. F. Durrant. Characterization of amorphous carbon films by PECVD and plasma ion implantation: the role of fluorine and sulfur doping, *Mater. Chem. Phys.* **227** (2019) 170-175.
[23] E. Kasparek, J. R. Tavares, M. R. Wertheimer, P-L. Girard-Lauriault, VUV photodeposition of thiol-terminated films: a wavelength-dependent study. *Langmuir* **34** (2018) 12234-12243